Direct observation of the NiTi martensitic phase transformation in nanoscale volumes

Jia Ye, Raj K. Mishra, Alan R. Pelton, Andrew M. Minor

Acta Materialia

2009

Final Accepted Version

Direct observation of the NiTi martensitic phase transformation in nanoscale volumes

Jia Ye[1], Raj K. Mishra[2], Alan R. Pelton[3], Andrew M. Minor[1]

[1]Department of Materials Science and Engineering, University of California, Berkeley and National Center for Electron Microscopy, Lawrence Berkeley National Laboratory, Berkeley, CA 94720

[2]General Motors Research and Development Center, Warren, MI 48090

[3]Nitinol Devices and Components, Fremont, CA 94539

Abstract

We report on quantitative *in situ* TEM nanocompression tests used to study the deformation behavior of NiTi pillars at the nanometer scale. By recording the diffraction patterns in real time we have obtained direct evidence that the stress-induced B2 to B19' (austenite to martensite) transformation does exist in NiTi even when the sample size is below 200 nm. Correlation of the appearance of the B19' phase in the diffraction pattern with our quantitative data showed that the transformation starts at approximately 1 GPa. We found that the transformation occurred through a multi-step process, and that the reverse transformation did not occur due to extensive deformation of the B19' phase. Our results have direct implications for the application of the shape memory effect in nanoscale NiTi devices.

Introduction

The shape memory effect [1] in Ni-Ti alloys is known to occur through a reversible martensitic phase transformation [2-12]. The basic shape memory phenomenon involves either a temperature-driven or stress-induced martensitic transformation that is then reversed by applying heat or stress reversal to reform the austenitic phase [13-20]. This basic transformation has been exploited in a number of different ways in order to develop advanced mechanical and biomedical devices [21-30].

As shape-memory technologies progress and these devices become smaller [31], questions remain as to whether or not the stress-induced martensitic phase transformation in NiTi progresses in the same manner or in fact exists at all when the critical dimensions approach nanometer scales. So far, mixed results have been reported. For instance, in references [32-34], no thermal martensitic phase transformation was found in nano-crystalline or thin film NiTi when the length-scale (grain size, thin film thickness) is roughly below 1 µm. Meanwhile, thermally-induced martensitic phase transformations in NiTi nano-powders [35] and stress-induced transformations in NiTi thin films by nano-indentation [36, 37] have both been reported. As an added complication, most of these reports use different sample geometries or different experimental methods, which can dramatically affect the results. Throughout these studies, there is universal concern about whether or not grain boundaries or a surface oxide layer hinders the martensitic phase transformation of NiTi at the nanometer scale.

Recently, Frick et al. [38] has extended the micropillar compression testing methodology that was first introduced by Uchic, et al. [39, 40] to the study of NiTi shape memory alloys. Using a Focused Ion Beam (FIB) to mill pillars of different diameters, they could study the compression behavior of different nominal sample sizes from the same starting materials. Using an instrumented *ex situ* nanoindenter, Frick, et al. compressed NiTi pillars ranging from 2 microns to 200 nm in diameter. By methodical analysis of their generated stress vs. strain curves, Frick et al. reported that the pseudoelastic behavior in NiTi disappeared when the pillar diameter became less than 200 nm. While the *ex situ* stress vs. strain curves generated from their experiments do show a lack of the pseudoelastic signature, they do not have direct microstructural analysis that demonstrates the vanishing pseudoelastic behavior in the smallest pillars. Thus, a main focal point of our work will be to examine whether the stress-strain curve resulting from a nanopillar compression test is indeed a valid proof of the existence of a phase transformation at small length scales.

Quantitative *in situ* TEM mechanical testing [41-43] is an ideal experimental method to directly probe the shape memory behavior of NiTi. By correlating mechanical data, the microstructural response and live crystallographic information we can explore the initial stages of deformation in this system at length scales that are difficult to approach with other testing methods. Here we present results from our *in situ* TEM uniaxial

nano-compression experiments of microfabricated NiTi pillar structures.

Materials and Methods

Our starting material was a NiTi thin film deposited using physical vapor deposition to a thickness of 5 μm with an austenite finish temperature (A_f) of 0 ˚C. At room temperature, the material has the austenite B2 phase and with grain sizes ranging from 200 to 500 nm. Figure 1a shows a regular TEM plan view image from the sample, prepared by traditional dimpling and Ar ion milling. The R phase was sometimes evident from diffraction patterns of the plan view samples, but was never observed in the pillar structures. An FEI 235 Dual Beam focused ion beam (FIB) was used to fabricate pillar structures with nominal diameters ranging from 140 nm to 200 nm and a length/diameter ratio between 2 and 3. A 20 nm thick amorphous/oxide layer was present around all the pillars (Fig.2(b)). More than 20 pillars were fabricated and tested. Due to the initial grain size of 200-400 nm, most pillars were single crystal but some contained one or two grain boundaries. *In situ* nano-compression of the pillars was performed with a Hysitron TEM Picoindenter system inside a JEOL 3010 TEM. An image of the experimental setup can be seen in Figure 1b, where a flat diamond punch approaches the pillar from the top in a direction normal to the electron beam. Most experiments used in this study were run under displacement control, while a few were run under force control, in order to be able to directly compare our results with prior work by others.

In addition to running tests in bright field and dark field TEM imaging modes, we also used an *in situ* diffraction mode in order to capture the phase transformation phenomena by observing the diffraction pattern during deformation instead of an image of the pillar. The diffraction patterns were obtained by placing a 270 nm diameter selected area diffraction aperture near the center of the pillar. As shown in Fig.2(a) inset, the diffraction pattern displays a strong amorphous ring caused by the FIB damage and/or oxidation. However, this amorphous ring can actually be used as a convenient reference to identify the phase transformation, since the first observable diffraction spot [110] of the B2 phase has nearly the same d-spacing as the amorphous ring. Consequently, any spots appearing inside the ring (e.g. d spacing less than the amorphous ring) indicate the appearance of a new phase. In the case of our experiments, any new spots would correspond to either the intermediate R phase or the martensite B19' phase. When running the experiment in diffraction mode we were able to easily synchronize the force-displacement data with the captured video by overlaying the data on the video, which can be seen in the supplementary movies.

Results and Discussion

1. The Martensitic Phase Transformation

The first important result we show here is that there is indeed a stress-induced

martensite phase transformation in sub-200 nm NiTi pillars. Fig. 2 shows a typical example. In this case, we started with a pillar from a single austenite B2 grain, and the diffraction pattern with a zone axis of [135] is shown in Fig.2(a) inset. After a single compression test to about 20% total engineering strain, the pillar was almost completely transformed to martensite B19', as shown in Fig.2(c) inset (the diffraction pattern was identified to be mostly B19' [001], with some residual B2 spots). Here, we define the engineering strain as the displacement of the punch divided by the initial length of the pillar taken from the TEM images. However, the actual strain induced in the material is difficult to measure accurately and as we will describe later includes complications from deformation in the substrate below. Nevertheless, it is useful to define a nominal value for comparison with other NiTi studies. Fig. 2(b) shows a high density of defects in the pillar to start, presumably largely due to damage from the FIB process. Fig. 2(d) shows the pillar after deformation, where there is a high density of defects surrounding the domain boundaries in the dark-field image - a common observation among the compressed pillars. We believe that the large amount of defects are generated to accommodate the formation of multiple B19' variants.

The *in situ* video of the diffraction pattern revealed the timing of the transformation process, as shown in Fig.3. Fig.3(a) shows the engineering stress vs. displacement curve of the aforementioned test. The stress was calculated with the initial pillar diameter from the top of the pillar, and this is consistent with all of the examples described in the paper. Due to a slight 3-4 degree taper of the pillar, this value therefore represents the highest stress imposed on the pillar at any given point. The first indication of the B2 to B19' phase transformation came at the plateau right before point (c), although the evidence of new diffraction spots is clearer at point (d). By position (e), the phase transformation was almost complete. The first feature worth noting is that, the phase transformation began at a stress level of about 1 GPa (a value that was consistent throughout all of our experiments). This value is higher than what is reported for bulk NiTi [44, 45], however comparable to Frick et al.'s results [38]. A second feature of interest is the subtle displacement jump at nearly constant load at point (c) corresponding to the first indication of the martensitic phase transformation. From evidence of the data alone it would be easy to confuse this subtle displacement excursion with underlying noise. With this in mind, it demonstrates that tracking the diffraction pattern for any changes is clearly a more reliable method for studying the martensite phase transformation than analysis of load vs. displacement features. A third feature of interest is that there are multiple steps and load plateaus during the loading of the pillar. For example, the load plateaus at both positions (c) and (e) in fig. 3(a) are qualitatively similar. Since the load plateaus are related to phase transformations, this indicates that the transformation of the pillar occurs in a multi-step process. The multi-step process is supported by the microstructural changes that were observed in the few tests we recorded in the dark field imaging mode. The idea of a multi-step transformation has been reported before in bulk samples [45, 46]. Finally, it is worth noting that the unloading curve shows a large "pop-out" following position (g). This kind of characteristic behavior has been used previously to identify the reversible

pseudoelasticity of NiTi alloys [38], indicative of the transformation back to the austenite B2 phase. However the diffraction patterns recorded before and after this "pop-out" are almost completely the same: both indicating a B19' phase. This apparent contradiction will be discussed in the next section.

The B19' diffraction patterns taken during and after the *in situ* compression tests always showed low-intensity streaking between the spots, suggesting that there are multiple B19' variants of small misorientation with each other that coexist after the tests. As for the intermediate R phase of NiTi, we did sometimes observe spots indicating its temporary existence before the B19' phase appeared. However the intensity of the presumed R phase diffraction spots was always too low to positively confirm from the *in situ* videos, and they were never found upon closer inspection after the tests.

As stated earlier, our nanopillars always had a thick amorphous layer surrounding them, presumably resulting from both FIB damage and subsequent oxidation. Nevertheless, our positive confirmation of the martensitic phase transformation allows us to conclude that the amorphous/oxide layer does not stop the transformation. On the other hand, we did observe that the phase transformation was stopped by grain boundaries when there were multiple grains within one pillar. These observations help to explain why it has been possible to observe the phase transformation in free-standing powders and pillars where oxide layers are bound to exist, but not in nano-crystalline bulk materials or thin films that contain multiple grain boundaries [32-37, 47, 48].

2. Reversibility

Pseudoelasticity is one of the characteristic properties of NiTi and occurs when there is full recovery of the phase transformation after unloading the imposed stress. It has been observed that for bulk NiTi, when the total strain is less than ~8%, the deformation is fully recoverable when testing is conducted at a temperature above A_f [14]. Here, we will take a look at the recoverability of the nanoscale NiTi pillars in our experimental setup.

For the example pillar used in Figures 2 and 3, about 20% maximum engineering strain was achieved. As shown by both the images and diffraction pattern taken after unloading, it is clear that the mechanical deformation was not fully recovered when the load was removed and the pillar remained in the B19' phase, as indicated in the previous section. As mentioned previously, there exists a high density of entangled dislocations in the final product, as shown in Fig.2(d).

As a comparison, another experiment was set up to load the pillar to a total engineering strain of about 15%, as shown in Fig.4. Both the load-displacement curve and the diffraction pattern indicate that the pillar, after a temporary partial transition to the B19' phase, fully recovered to the original B2 phase, as well as to its original length. By further compressing the pillar beyond 20% strain, the deformation again became partly

unrecoverable (Fig.5).

Our understanding of this behavior is that in pseudoelastic NiTi, the first 10% nominal strain is accommodated by martensite phase transition. Beyond this limit, the dislocations start to move in the B19' phase and the deformation becomes permanent. When the sample has deformed significantly the resulting dislocation entanglement in the B19' phase will hinder the reverse phase transformation to the B2 phase [49-51]. The lack of reversibility in the pillars compressed to 20% nominal engineering strain was confirmed by heating the compressed pillars. After compressing a series of pillars to 20% nominal engineering strain and confirming the B19' phase was stable, we took

the sample outside of the microscope and heat treated the pillars for 15 minutes at 100 °

C. This temperature is well above the A_f and should have been sufficient to transform bulk NiTi back to the austenite phase. After re-inserting the sample into the TEM we found that the microstructure remained exactly the same, confirming that the pillars remained in the B19' phase after compression to 20% engineering strain.

At first glance, the shape of the engineering stress vs. displacement curves that we measured from the *in situ* nanocompression tests seem to indicate the presence of pseudoelasticity. Pseudoelasticity as observed in nanoindentation and nanocompression tests is normally signified by a hysteretic stress vs. strain curve, resulting from the forward and reverse phase transformation at a relatively constant load [52]. Our data curves also demonstrated similar features, including small "pop-ins" and pronounced "pop-outs" upon unloading (Fig.3a for example). However, the lack of a reverse phase transformation in the pillar confirmed by the diffraction information taken from the pillars seemed entirely inconsistent with this interpretation of the pop-out behavior. To look for the origin of this pop-out behavior, we ran *in situ* compression tests using the bright field imaging mode. As opposed to recording the tests in dark field or in diffraction mode, the bright field imaging mode allowed us to observe the profile of the substrate below the pillars. Analysis of our bright field tests indicated that the pronounced "pop-out" features during unloading were in fact a result of substantial deformation and recovery in the substrate below the pillars, a unique feature to the NiTi pillars as compared to our previous in situ nanocompression tests on other non-shape memory systems [43, 53-55]. In Fig.6 we show a bright field test run in displacement control and in Fig.7 we show a bright field test run under force control. In both cases, the "pop out" of the substrate below the pillar accounted for approximately 90% of the total "pop out". During the compression tests, the stress in the substrate must be much smaller than the stress in the pillars, but evidently the stress is large enough in the substrate to result in a reversible transformation. While the pillars are fully transformed to B19' phase, which is locked into the pillar through subsequent plasticity, the substrates is likely only partially transformed, resulting in at least a partially reversible transformation. It has been found before that the phase transformation in shape memory alloys can be enhanced by a triaxial stress state, such as at the corner of the gage section in dog-bone shaped tensile samples [56-58]. This is

consistent with the phase transformation occurring at much lower stress in the substrate below the pillars in our experiments.

While our *in situ* diffraction data came from the pillars only, the quantitative data is evidently a superposition of the deformation in the pillars and the substrate below. Our quantitative data has features that are clearly derived from deformation in the pillar itself (as described in Figure 2 for example), but there is underlying deformation in the substrate below that leads to inflated strain values, since some displacement is derived from the substrate. This observation also helps to explain why we found a fully reversible transformation at approximately 15% nominal engineering strain (Figure 4) instead of at 8% strain as is reported for bulk tests. This becomes yet another example of the power of *in situ* observations in helping to interpret quantitative data. For example, a recent paper claims that at the nanoscale Cu-Al-Ni shape memory alloys show a damping figure of merit that is much higher than the value for their bulk counterpart[59]. Their conclusion was drawn from *ex situ* nanopillar compression tests, based on an assumption that the deformation was localized within the pillars. As our *in situ* results clearly show, it is possible that the deformation can extend into the substrate. Although the authors of this recent paper were using a different alloy system than ours, the mechanical behavior of these shape memory alloys is similar. If the deformation of the Cu-Al-Ni nanopillars indeed extended into the substrate as shown in our work, then their calculation of the damping figure of merit using only the volume of the pillar would be incorrect. This example clearly shows the importance of *in situ* work for the interpretation of small-scale mechanical testing and the development of nanoscale applications.

Summary

We have used quantitative *in situ* TEM nanocompression tests to study the stress-induced martensitic phase transformation in NiTi at the nanometer scale. We obtained direct evidence that the stress-induced B2->B19' (austenite to martensite) transformation does exist in NiTi even when the sample size is below 200 nm. Correlation of the appearance of the B19' phase in the diffraction pattern with our quantitative data showed that the transformation starts at about 1 GPa. We found that the transformation occurred through a multi-step process, indicating sequential nucleation of martensitic variants at progressively higher stresses. When the nominal engineering strain value exceeded 20%, the transformation in our nanopillars was not reversible, even after subsequent heat treatment. However, we found that features indicative of pseudoelasticity in the nanopillars in fact resulted from movement (and presumably pseudoelastic behavior) of the substrate below the pillars. Although there is no clear evidence due to the resolution of our current experimental setup, we have clues that indicate the temporary existence of the intermediate R phase. While our study suggests the potential for applications of the shape memory effect in nanoscale NiTi devices, it also calls for further studies, especially into the role of the R phase and cyclic behavior.
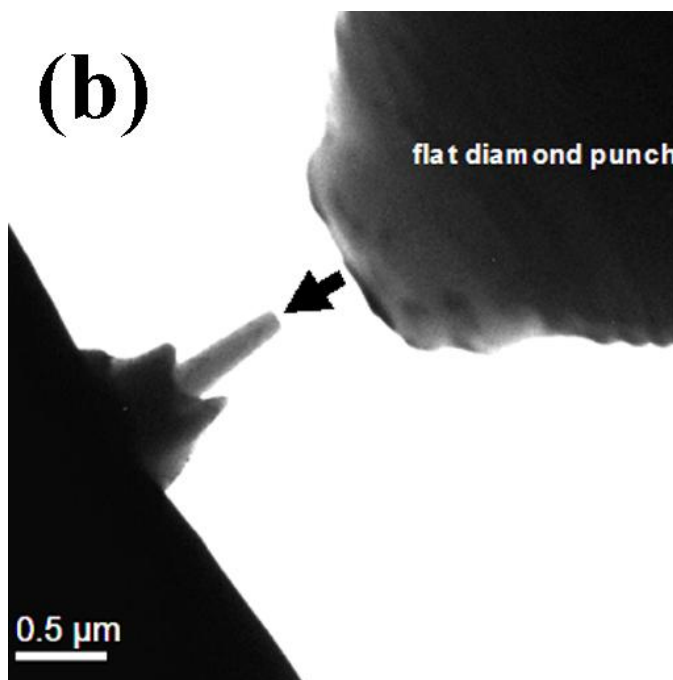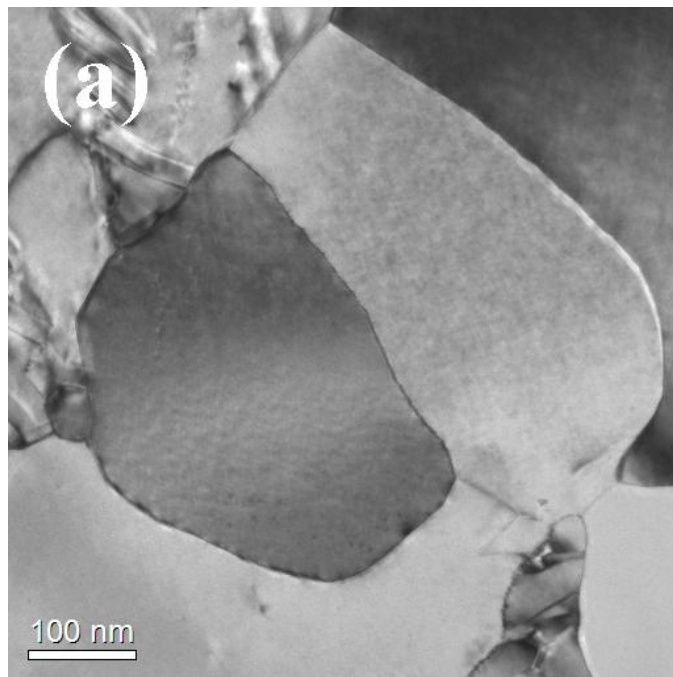
Figures

Figure 1. (a) Planview of NiTi thin film; (b) Low magnification TEM image showing *in situ* nano-compression experimental setup.
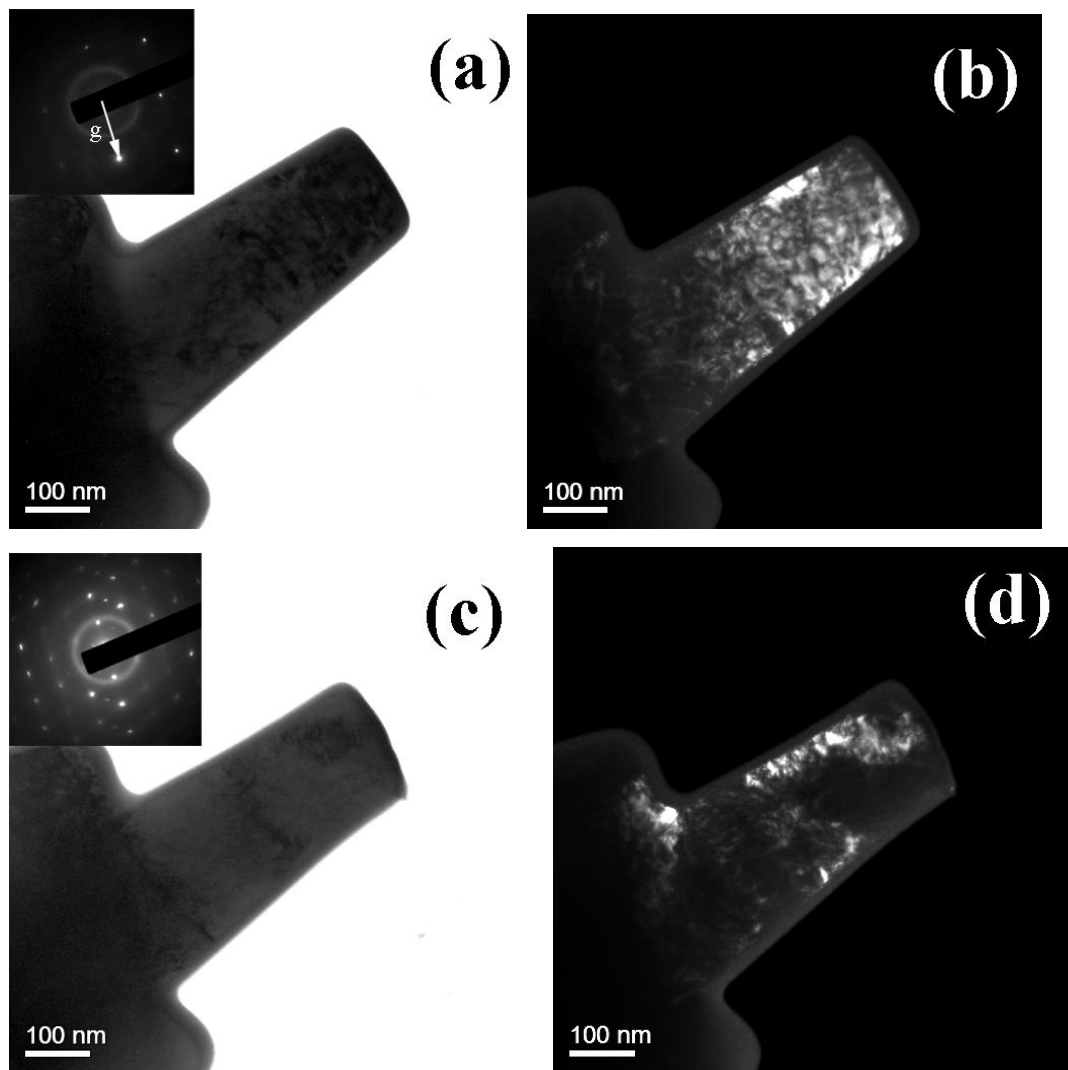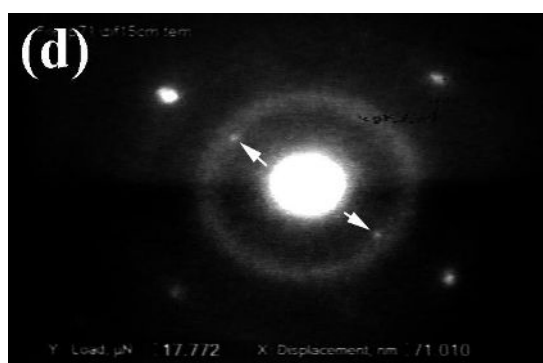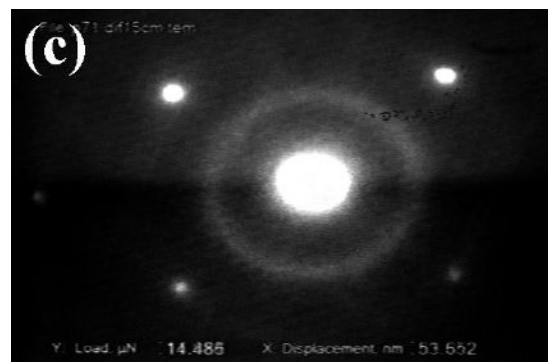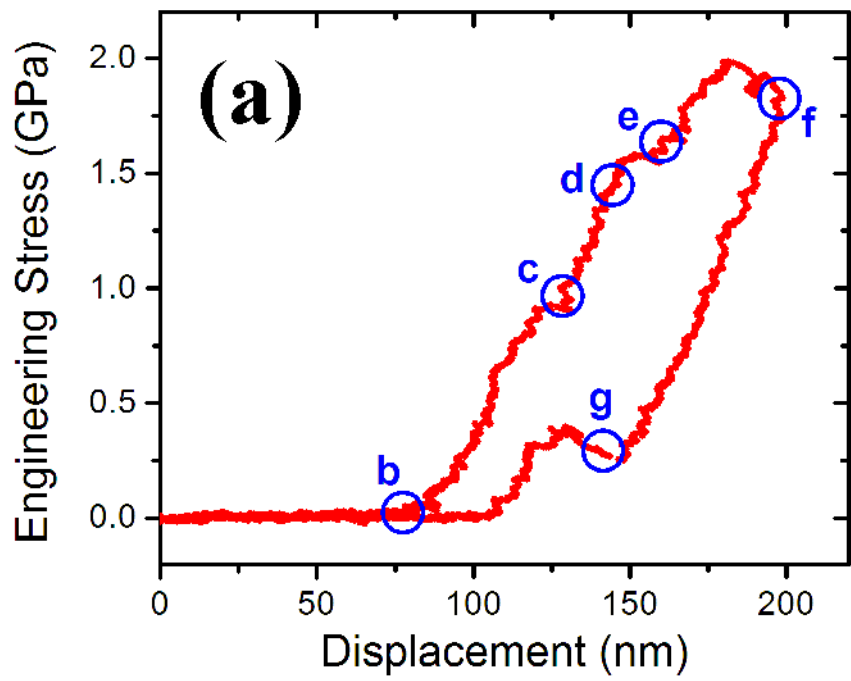
Figure 2. Representative before and after microstructure from a NiTi pillar compressed *in situ* in a TEM to approximately 20% engineering strain. (a) Bright-field and (b) dark-field images of a FIB-milled NiTi pillar before testing. The diffraction pattern inset in (a) show that the pillar is a single crystal of the austenite cubic B2 phase, and the diffraction spot used for the dark-field image (b) was g=B2[-2-11]. (c) and (d) are bright-field and dark field images, respectively, of the same pillar after-compression. The spot used for the dark-field images was the same g=B2[-2-11], now overlapping with the B19' [-2,-2,0] diffraction spot. The pillar has been mostly transformed to the B19'phase, shown by the inset diffraction pattern in (c).

(a)

(b) Y. Load, μN 0.201 X. Displacement, nm 41.028

(c) Y. Load, μN 14.486 X. Displacement, nm 53.652

(d) Y. Load, μN 17.772 X. Displacement, nm 71.010

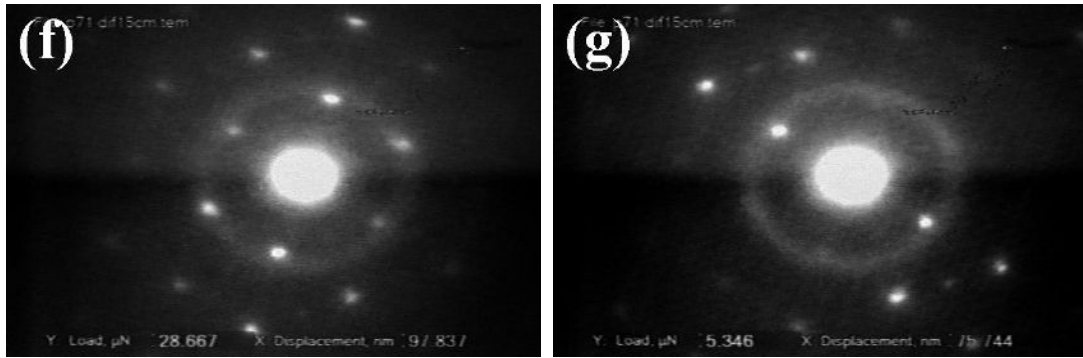(e) Y. Load, μN 26.614 X. Displacement, nm 85.213

Figure 3. (a) Engineering stress vs. displacement curve of the test shown in Fig.1. The video frames (b-g) correspond to the points marked on (a), and in each case the diffraction pattern corresponding to the end of an event is shown in order to show the full intensity of the newly transformed phase. The diffraction pattern shown in (b) corresponds to the austenite B2 phase only. The B2 -> B19' phase transformation begins at the plateau right before point (c) and is fully transformed by point (f). The first characteristic B19' diffraction spots are marked by arrows in (d), but can also be seen in the subsequent diffraction patterns as can the appearance of additional B19' spots.
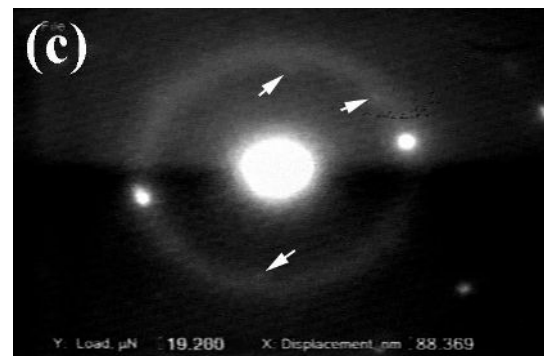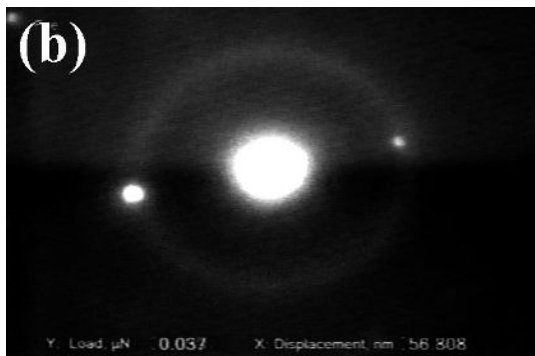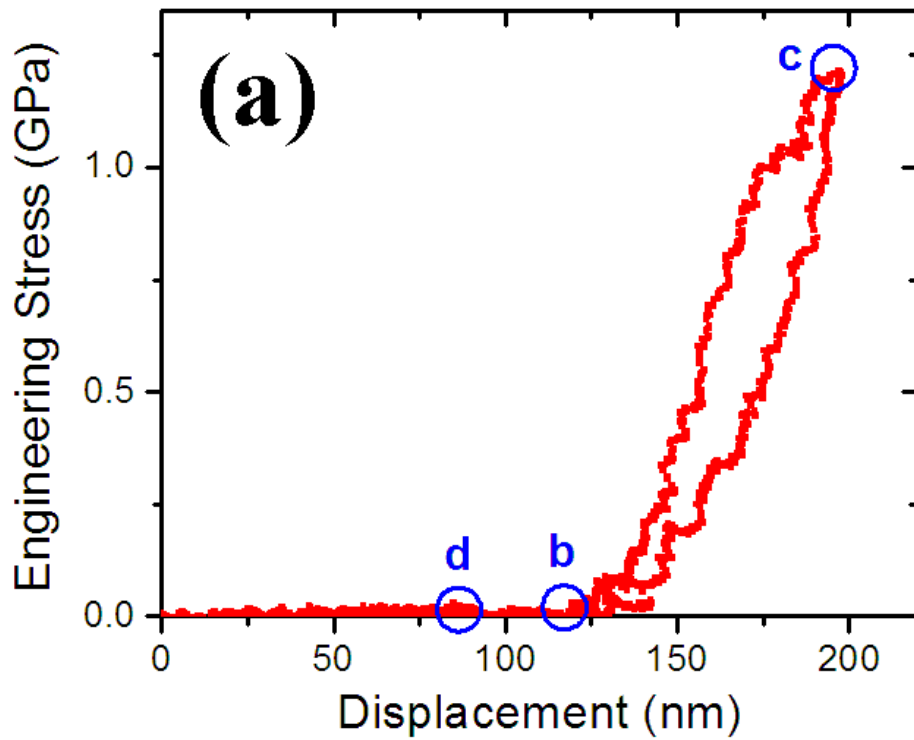
Fig.4 Engineering stress vs. displacement curve (a) and corresponding diffraction patterns (b-d) from a compression test with 15% nominal engineering strain. The video frames (b-d) correspond to the points marked on (a), and in each case the frame corresponding to the end of an event in shown in order to show the full intensity of the

newly transformed phase. The diffraction pattern at the beginning of the loading segment (b) shows only the austenite B2 phase. The arrows in (c) highlight the appearance of diffraction spots that correspond to martensite B19' phase, but these disappear upon unloading, shown in (d).
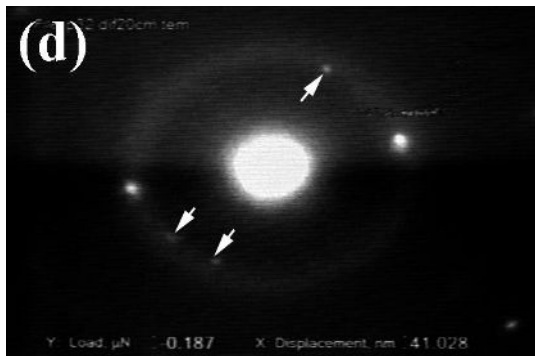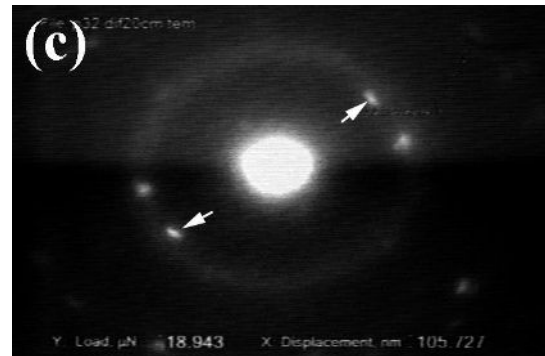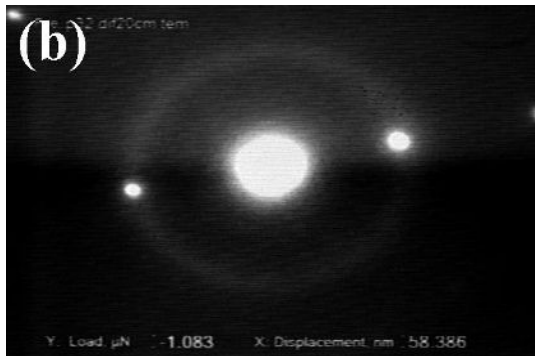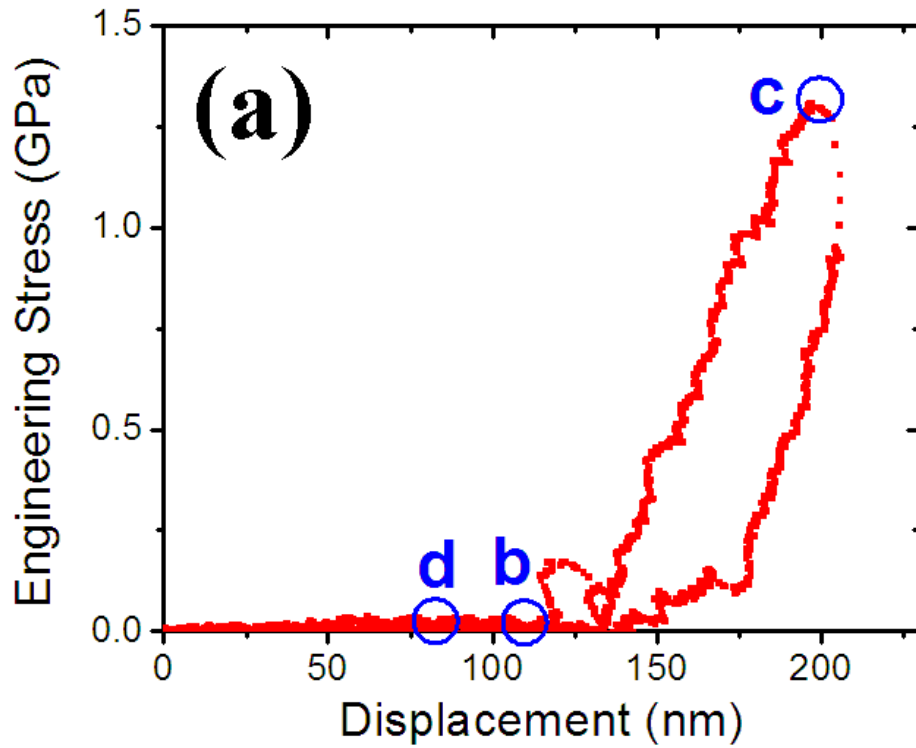
Fig.5 Engineering stress vs. displacement curve (a) and corresponding diffraction patterns (b-d) of a compression test with 20% nominal engineering strain following the test shown in Fig.3. The video frames (b-d) correspond to the points marked on (a), and in each case the frame corresponding to the end of an event is shown in order to show

the full intensity of the newly transformed phase. The diffraction pattern (c) shows only the austenite B2 phase exists before the test. The arrows in (c) highlight the appearance of diffraction spots that correspond to the martensite B19' phase. After unloading the B19' spots still exist, shown by the arrows in (d), as opposed to the test in Fig. 4.
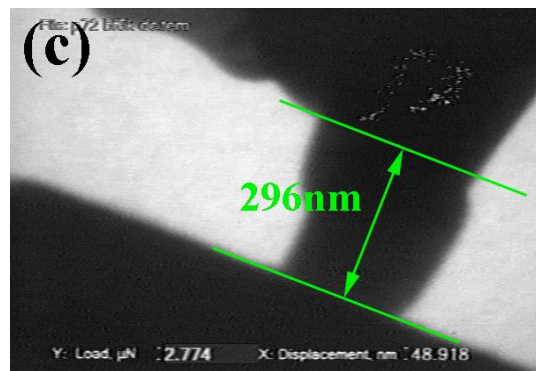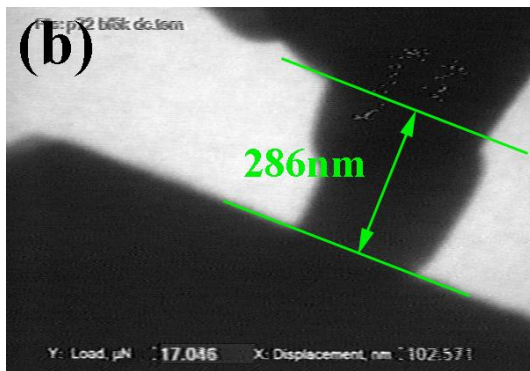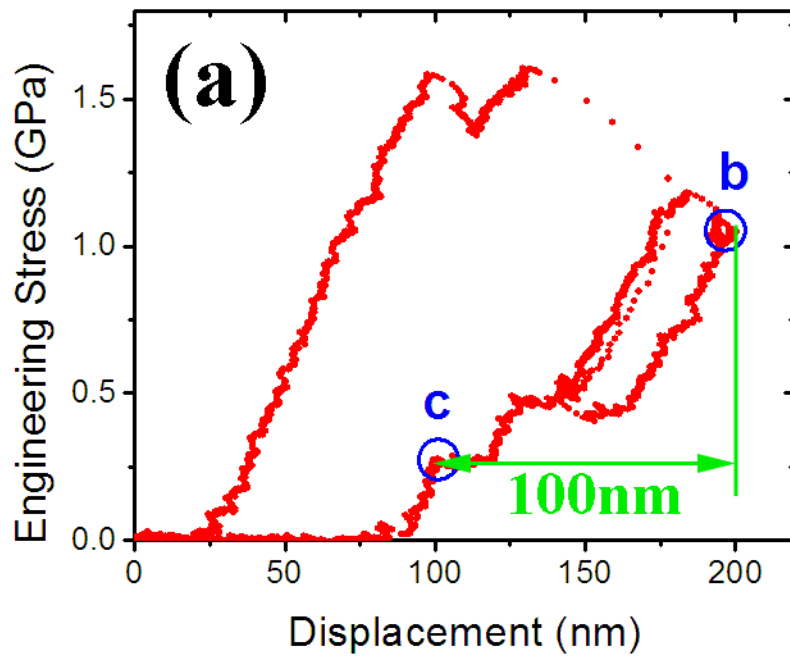
Fig.6 A displacement-controlled test performed while recording the bright-field image shows that 90% of the pop-out comes from the substrate. In (a) the engineering stress vs. displacement curve shows that over the 100 nm of unloading displacement between points (b) and (c) the pillar only expanded by 10 nm.
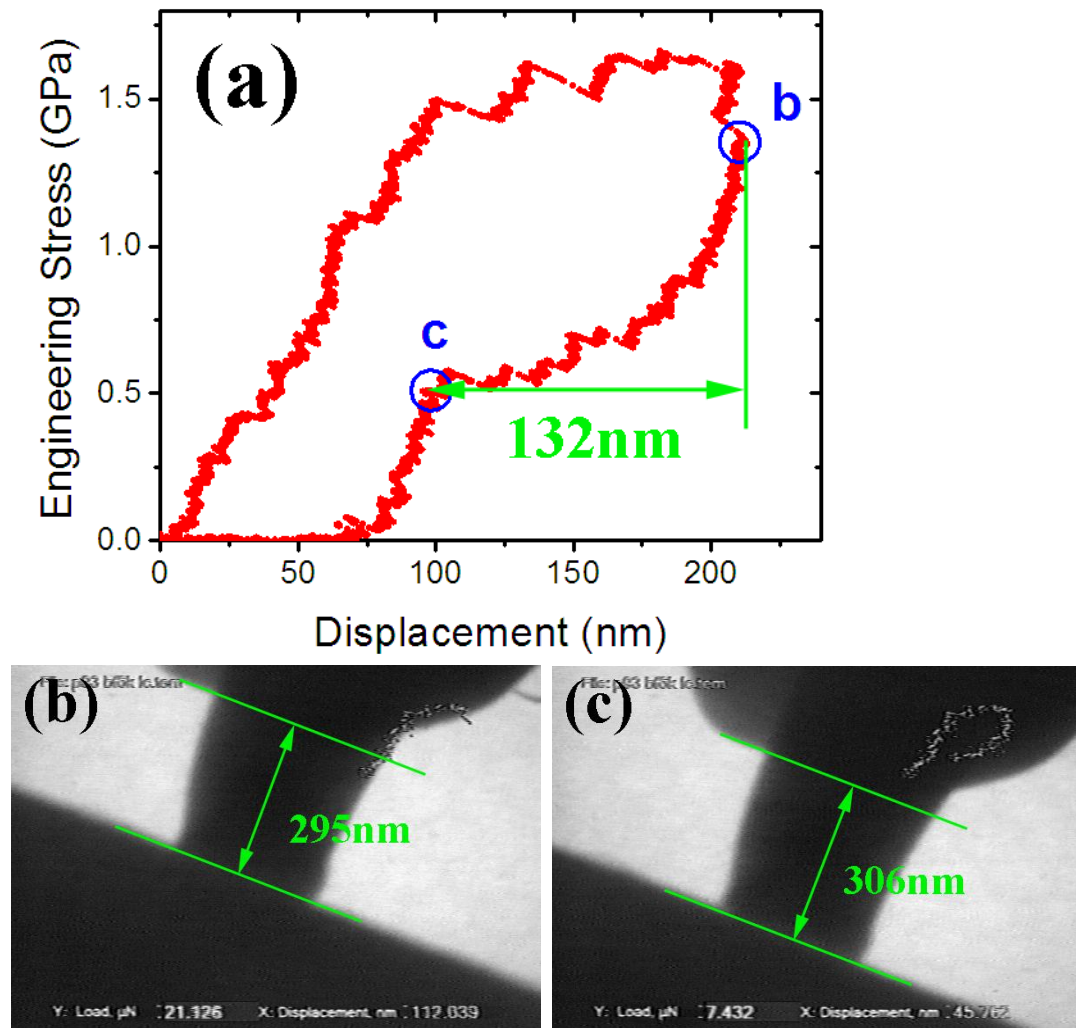
Fig.7 A load-controlled test performed while recording the bright-field image shows that 92% of the pop-out comes from the substrate. In (a) the engineering stress vs. displacement curve shows that over the 132 nm of unloading displacement between points (b) and (c) the pillar only expanded by 12 nm.

References

[1]   Buehler WJ, Wiley RC, Gilfrich JV. Effect of Low-Temperature Phase Changes on Mechanical Properties of Alloys near Composition Tini. J. Appl. Phys. 1963;34:1475.

[2]   Otsuka K, Ren X. Physical metallurgy of Ti-Ni-based shape memory alloys. Progress in Materials Science 2005;50:511.

[3]   Wasilews.Rj, Butler SR, Hanlon JE, Worden D. Homogeneity Range and Martensitic Transformation in Tini. Metallurgical Transactions 1971;2:229.

[4]   Koskimak.D, Marcinko.Mj, Sastri AS. Solid State Diffusional Transformations in near-Equiatomic Ni-Ti Alloys. Transactions of the Metallurgical Society of Aime 1969;245:1883.

[5]   Nishida M, Wayman CM, Honma T. Precipitation Processes in near-Equiatomic Tini Shape Memory Alloys. Metallurgical Transactions a-Physical Metallurgy and Materials Science 1986;17:1505.

[6]   Otsuka K, Sawamura T, Shimizu K, Wayman CM. Characteristics of Martensitic Transformation in Tini and Memory Effect. Metallurgical Transactions 1971;2:2583.

[7]   Otsuka K, Sawamura T, Shimizu K. Crystal Structure and Internal Defects of Equiatomic Tini Martensite. Phys. Status Solidi A-Appl. Res. 1971;5:457.

[8]   Hehemann RF, Sandrock GD. Relations between Premartensitic Instability and Martensite Structure in Tini. Scripta Metallurgica 1971;5:801.

[9]   Michal GM, Sinclair R. The Structure of Tini Martensite. Acta Crystallogr. Sect. B-Struct. Commun. 1981;37:1803.

[10] Buhrer W, Gotthardt R, Kulik A, Mercier O, Staub F. Powder Neutron-Diffraction Study of Nickel Titanium Martensite. Journal of Physics F-Metal Physics 1983;13:L77.

[11] Kudoh Y, Tokonami M, Miyazaki S, Otsuka K. Crystal-Structure of the Martensite in Ti-49.2 at-Percent-Ni Alloy Analyzed by the Single-Crystal X-Ray-Diffraction Method. Acta Metallurgica 1985;33:2049.

[12] Miyazaki S, Otsuka K. Development of Shape Memory Alloys. ISIJ Int. 1989;29:353.

[13] Ling HC, Kaplow R. Stress-Induced Shape Changes and Shape Memory in the R and Martensite Transformations in Equiatomic Niti. Metallurgical Transactions a-Physical Metallurgy and Materials Science 1981;12:2101.

[14] Saburi T, Yoshida M, Nenno S. Deformation-Behavior of Shape Memory Ti-Ni Alloy Crystals. Scripta Metallurgica 1984;18:363.

[15] Miyazaki S, Otsuka K. Deformation and Transition Behavior Associated with the R-Phase in Ti-Ni Alloys. Metallurgical Transactions a-Physical Metallurgy and Materials Science 1986;17:53.

[16] Stachowiak GB, McCormick PG. Shape Memory Behavior Associated with the R and Martensitic Transformations in a Niti Alloy. Acta Metallurgica 1988;36:291.

[17] Miyazaki S, Wayman CM. The R-Phase Transition and Associated Shape Memory Mechanism in Ti-Ni Single-Crystals. Acta Metallurgica 1988;36:181.

[18] Shaw JA, Kyriakides S. Thermomechanical Aspects of Niti. Journal of the Mechanics and Physics of Solids 1995;43:1243.

[19] Shaw JA, Kyriakides S. On the nucleation and propagation of phase transformation fronts in a NiTi alloy. Acta Materialia 1997;45:683.

[20] Eggeler G, Hornbogen E, Yawny A, Heckmann A, Wagner M. Structural and functional fatigue of NiTi shape memory alloys. Mater. Sci. Eng. A-Struct. Mater. Prop. Microstruct. Process. 2004;378:24.

[21] Fu YQ, Du HJ, Huang WM, Zhang S, Hu M. TiNi-based thin films in MEMS applications: a review. Sensors and Actuators a-Physical 2004;112:395.

[22] Benard WL, Kahn H, Heuer AH, Huff MA. Thin-film shape-memory alloy actuated micropumps. Journal of Microelectromechanical Systems 1998;7:245.

[23] Krulevitch P, Lee AP, Ramsey PB, Trevino JC, Hamilton J, Northrup MA. Thin film shape memory alloy microactuators. Journal of Microelectromechanical Systems 1996;5:270.

[24] Ishida A, Martynov V. Sputter-deposited shape-memory alloy thin films: Properties and applications. Mrs Bulletin 2002;27:111.

[25] Kahn H, Huff MA, Heuer AH. The TiNi shape-memory alloy and its applications for MEMS. Journal of Micromechanics and Microengineering 1998;8:213.

[26] Lee AP, Ciarlo DR, Krulevitch PA, Lehew S, Trevino J, Northrup MA. A practical microgripper by fine alignment, eutectic bonding and SMA actuation. Sensors and Actuators a-Physical 1996;54:755.

[27] Duerig T, Pelton A, Stockel D. An overview of nitinol medical applications. Elsevier Science Sa, 1999. p.149.

[28] Chu CL, Hu T, Wu SL, Dong YS, Yin LH, Pu YP, Lin PH, Chung CY, Yeung KWK, Chu PK. Surface structure and properties of biomedical NiTi shape memory alloy after Fenton's oxidation. Acta Biomater. 2007;3:795.

[29] Chu CL, Chung CY, Lin PH, Wang SD. Fabrication of porous NiTi shape memory alloy for hard tissue implants by combustion synthesis. Mater. Sci. Eng. A-Struct. Mater. Prop. Microstruct. Process. 2004;366:114.

[30] Morgan NB. Medical shape memory alloy applications - the market and its products. Elsevier Science Sa, 2004. p.16.

[31] Bhattacharya K, James RD. The material is the machine. Science 2005;307:53.

[32] Ishida A, Sato M. Thickness effect on shape memory behavior of Ti-50.0at.%Ni thin film. Acta Materialia 2003;51:5571.

[33] Waitz T, Kazykhanov V, Karnthaler HP. Martensitic phase transformations in nanocrystalline NiTi studied by TEM. Acta Materialia 2004;52:137.

[34] Fu YQ, Zhang S, Wu MJ, Huang WM, Du HJ, Luo JK, Flewitt AJ, Milne WI. On the lower thickness boundary of sputtered TiNi films for shape memory application. Thin Solid Films 2006;515:80.

[35] Fu YQ, Shearwood C. Characterization of nanocrystalline TiNi powder. Scripta Materialia 2004;50:319.

[36] Shaw GA, Trethewey JS, Johnson AD, Drugan WJ, Crone WC. Thermomechanical high-density data storage in a metallic material via the shape-memory effect. Advanced Materials 2005;17:1123.

[37] Frick CP, Lang TW, Spark K, Gall K. Stress-induced martensitic transformations and shape memory at nanometer scales. Acta Materialia 2006;54:2223.

[38] Frick CP, Orso S, Arzt E. Loss of pseudoelasticity in nickel-titanium sub-micron compression pillars. Acta Materialia 2007;55:3845.

[39] Uchic MD, Dimiduk DM, Florando JN, Nix WD. Sample dimensions influence strength and crystal plasticity. Science 2004;305:986.

[40] Dimiduk DM, Woodward C, LeSar R, Uchic MD. Scale-Free Intermittent Flow in Crystal Plasticity. Science 2006;312:1188.

[41] Minor AM, Asif SAS, Shan ZW, Stach EA, Cyrankowski E, Wyrobek TJ, Warren OL. A new view of the onset of plasticity during the nanoindentation of aluminium. Nature Materials 2006;5:697.

[42] Sun Y, Ye J, Shan Z, Minor AM, Balk TJ. The mechanical Behavior of nanoporous gold thin films. Jom 2007;59:54.

[43] Shan ZW, Mishra RK, Asif SAS, Warren OL, Minor AM. Mechanical annealing and source-limited deformation in submicrometre-diameter Ni crystals. Nature Materials 2008;7:115.

[44] Rozner AG, Wasilews.Rj. Tensile Properties of Nial and Niti. Journal of the Institute of Metals 1966;94:169.

[45] Miyazaki S, Otsuka K, Suzuki Y. Transformation Pseudo-Elasticity and Deformation-Behavior in a Ti-50.6at-Percent Ni-Alloy. Scripta Metallurgica 1981;15:287.

[46] Bataillard L, Bidaux JE, Gotthard R. Interaction between microstructure and multiple-step transformation in binary NiTi alloys using in-situ transmission electron microscopy observations. Philos. Mag. A-Phys. Condens. Matter Struct. Defect Mech. Prop. 1998;78:327.

[47] Waitz T, Spisak D, Hafner J, Karnthaler HP. Size-dependent martensitic transformation path causing atomic-scale twinning of nanocrystalline NiTi shape memory alloys. Europhysics Letters 2005;71:98.

[48] Waitz T, Antretter T, Fischer FD, Simha NK, Karnthaler HP. Size effects on the martensitic phase transformation of NiTi nanograins. Journal of the Mechanics and Physics of Solids 2007;55:419.

[49] Xie ZL, Liu Y, Van Humbeeck J. Microstructure of NiTi shape memory alloy due to tension-compression cyclic deformation. Acta Materialia 1998;46:1989.

[50] Ma XG, Komvopoulos K. Nanoscale pseudoelastic behavior of indented titanium-nickel films. Appl. Phys. Lett. 2003;83:3773.

[51] Ni WY, Cheng YT, Grummon DS. Recovery of microindents in a nickel-titanium shape-memory alloy: A "self-healing" effect. Appl. Phys. Lett. 2002;80:3310.

[52] Liu Y, Xie Z, Van Humbeeck J, Delaey L. Asymmetry of stress-strain curves under tension and compression for NiTi shape memory alloys. Acta Materialia 1998;46:4325.

[53] Shan ZW, Li J, Cheng YQ, Minor AM, Asif SAS, Warren OL, Ma E. Plastic flow and failure resistance of metallic glass: Insight from in situ compression of nanopillars. Physical Review B 2008;77.

[54] Sriram V, Yang JM, Ye J, Minor AM. Determining the stress required for deformation twinning in nanocrystalline and ultrafine-grained copper. Jom 2008;60:66.

[55] Ye J, Mishra RK, Minor AM. Relating nanoscale plasticity to bulk ductility in aluminum alloys. Scripta Materialia 2008;59:951.

[56] Gall K, Sehitoglu H, Maier HJ, Jacobus K. Stress-induced martensitic phase transformations in polycrystalline CuZnAl shape memory alloys under different stress states. Metallurgical and Materials Transactions a-Physical Metallurgy and Materials Science 1998;29:765.

[57] Jacobus K, Sehitoglu H, Balzer M. Effect of stress state on the stress-induced martensitic transformation in polycrystalline Ni-Ti alloy. Metallurgical and Materials Transactions a-Physical Metallurgy and Materials Science 1996;27:3066.

[58] Huang MS, Gao XJ, Brinson LC. A multivariant micromechanical model for SMAs Part 2. Polycrystal model. Int. J. Plast. 2000;16:1371.

[59] Juan JS, No ML, Schuh CA. Nanoscale shape-memory alloys for ultrahigh mechanical damping. Nat Nano 2009;advanced online publication.